Final Report

NASA JRI Contract #NCC2-5067

Optical Design of Plant Canopy Measurement System and Fabrication of Two-Dimensional High-Speed Metal-Semiconductor-Metal Photodetector Arrays

Anthony Sarto, Bart Van Zeghbroeck, and Vern C. Vanderbilt

1. Overview

Under the NASA JRI Contract #NCC2-5067, we have assisted in the electrical and optical design of a prototype plant canopy architecture measurement system being developed by Vern C. Vanderbilt at NASA-Ames Research Center. The design is initially intended to provide a working testbed system, similar to the system developed here at the University of Colorado, for system studies at NASA-Ames Research Center. This design will then be implemented into a Controlled Ecological Life Support System (CELSS) currently employed at NASA-Ames Research Center. The completed electrical and optical designs include specified component and parts lists.

The second task of this contract was to design and fabricate two-dimensional (2-D) metal-semiconductor-metal (MSM) photodiode arrays. However, continued testing of the single detector based system at the University of Colorado indicated that there were several areas with respect to measurement sensitvity that needed to be investigated. Discussions with Dr. Vanderbilt led to the conclusion that it was more useful to address these more fundamental sensitivity issues, rather than move towards more system complexity resulting from the implementation of 2-D arrays. Therefore instead of designing and fabricating 2-D arrays we have conducted system studies and outlined several means by which to increase the sensitivity of the plant canopy architecture measurement system. In this light, we have also fabricated several single element MSM detectors which we consider to have superior performance to the previous generation of detectors, and have included these detectors as deliverables instead of 2-D arrays. The following end items have been provided for this contract:

1) Electrical and optical designs for the prototype plant canopy architecture measurement system, including specified component and parts lists.

2) 6 single MSM detectors mounted in high-speed packages.

3) This final report.

2. Plant canopy architecture measurement system design

2.1 Optical subsystem design

The concept of the optical subsystem is quite simple: deliver a short optical pulse to the canopy, and collect the scattered light from the canopy using a high-bandwidth detector detector, which combined with a correlation processing method, allows a measure of canpy reflectivity versus depth. This is essentially a lidar ranging application, and in concept is quite straightforward. The key aspects of the testbed and CELSS design which must be considered in the design are the following:

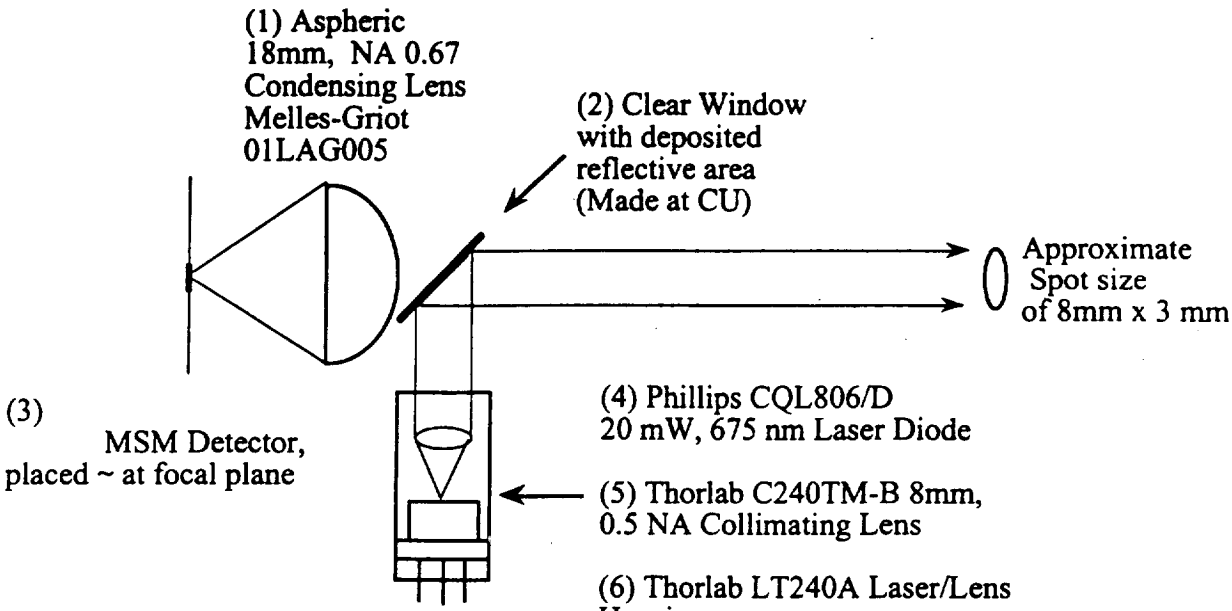

Figure 1. A simple optical design for the plant canopy architecture measurement system. The design is essentially identical to the as-built system at The University of Colorado.

• The testbed and the intended CELSS system are relatively short in length in terms of creating a far field collection condition when implemented with typical lens focal lengths. As a

result the object is not really in the far field and therefore the collection problem is still essentially an imaging problem, where the image size can vary considerably over the intended range of plant canopy depths (approximately 0.2 to 1 meter).

• The MSM photodetectors are very small (50 x 50μ up to 200 x 200μ) which requires a very short effective focal length system in order to image an adequate (approximately 1 cm diameter) sized spot onto the detector over a large range of canopy depth. The small detector size requires careful alignment of the optical system.

• With the laser sources used to date, the reflected energy off diffuse targets is small and as large a collection aperture as possible is desired.

• The transmit and receive optics must ultimately fit into a very compact housing for implementation into the CELSS system.

• This is a power limited problem.

This translates into the requirement to design a very short focal length system with the highest possible N.A. (low f/#). This was the approach taken in the design shown below in figure 1. The design is extremely simple, using only a single aspheric lens with a very high N.A. of 0.67 (focal length of 18mm, aperture of 24.2mm). This enables an approximately 8mm x 3mm canopy illumination spot onto a 200μ x 200μ MSM detector, over a canopy depth range of approximately 0.75m to 1.5m. A single lens is sensible (as opposed to a multi-lens system) from the standpoint of simplicity and compactness for this application, and because the actual image quality is not important. While a larger aperture would increase the optical collection area, compactness is a primary issue here. The Melles-Griot lens identified in the figure was the highest of the shelf N.A.

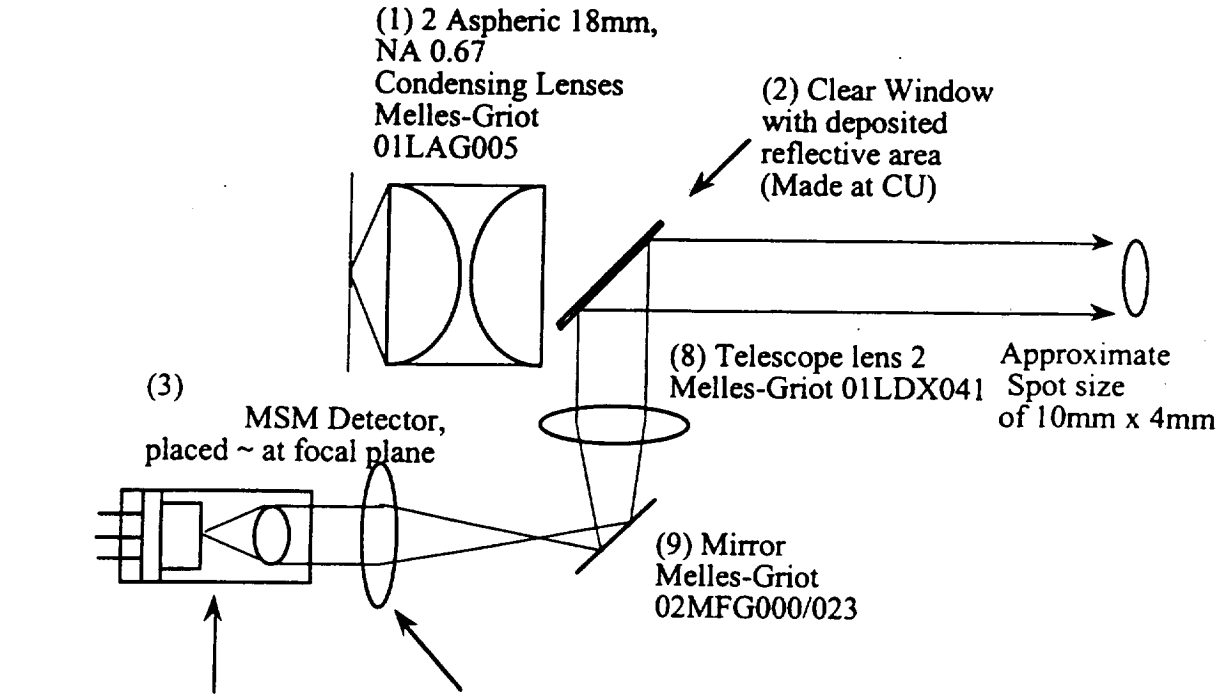

Figure 2. Alternative optical design with shorter effective focal length allowing the use of a larger canopy illumination spot size.

lens that was available. The reflector combiner shown in figure 1 is a transparent plate with a reflective portion deposited on it. The reflective spot on the plate is the same size as the desired canopy illumination spot size. This method of injecting the canopy illumination beam is superior to using a beamsplitter (approximately 3dB) because there is no loss incurred while launching the beam. The return collection losses are also lower than that when using a beamsplitter, essentially proportional to the ratio of the reflective spot size area to the lens aperture area. In the current system at the University of Colorado, the loss is on the order of 1dB. An additional advantage to this approach is that the output spot size is independent of any of the collection optics, for example in terms of beam-splitter aperture or collection lens alignment. Using a polarizing beamsplitter could is conceivable, especially since the laser diode is polarized, however the polarization of the reflected return illumination is not predicatble.

The design shown in figure 2 uses two of the Melles-Griot high N.A. lenses to create a reduced effective focal length of approximately 11.5mm. As shown, this would allows imaging a larger sized spot onto the detector, or alternatively, a closer minimum imaging distance. A telescope is used to increase the spot size. It is possible that imaging characteristics of the double lens combination will be somewhat aberrated however. The folding mirror use in the telescope is optional, introduced to make the system more compact. Parts lists for the designs shown in figures 1 and 2 are included in Appendix A.

The designs shown in figures 1 and 2 are drawn approximately full-scale, and the CELSS application would involve constructing a detector head assembly, accomplished by placing these components in a small, environmentally protected enclosure. Primarily because of the small detector size, the optical component alignment is critical. The testbed layout implemented at The University of Colorado is essentially the same design as that of figure 1, where the testbed has an additional imaging system comprised of the beamsplitter, lens, and CCD camera. The imaging system is made by placing a beamsplitter in between the reflective output coupling mirror and the high N.A. lens, and then imaging the detector onto the CCD camera with another lens. The imaging system enables the position of the image of the spot to be properly aligned on the MSM detector. Such an imaging system would be very useful to implement during the construction/alignment phase of the CELSS detector head assembly.

An alternative approach to consider for a detector head assembly would be a small Cassegrain-type telescope design. It is possible that a higher N.A. system could be with such an approach, although the near-field aspect of the CELSS application may make this approach difficult. Employing plastic optics may allow for higher N.A. lenses.

2.2 Plant canopy architecture measurement system electrical design

2.2.1 Electrical driver circuits

The electrical subsystem design is shown in the upper portion of figure 3, and the corresponding electrical parts-list is provided in Appendix A. This circuit has been built at The University of Colorado. It is capable of producing electrical and optical pulses on the order of 50 picoseconds in length at a rate of approximately 100 MHz. The correlation measurement scheme correlates an input electrical pulse to the MSM detector with a reflected optical pulse from the canopy, also incident on the MSM detector. There are two branches to the circuit, one branch, the laser diode driver circuit (the upper branch shown in the figure) creates the electrical pulse which sits on a DC bias for input to the laser diode which produces a short optical pulse via a laser relaxation oscillation. The other branch, the MSM driver circuit, (the lower branch in the figure) creates the variable-delay electrical pulse which rides on a DC bias for input into the MSM. As described in the final report for the previous JRI Contract #NCA2-788, the circuit comprised of R_{int} and C_{int} acts as a simple RC integrator circuit, with no amplification. At present, the circuit capacitance C_{int} is the intrinsic capacitance of a 50Ω coax transmission line (typically 100 picofarads), and R_{int} is the resistance of the internal current source (approximately 1 MΩ) provided by an HP parameter analyzer. Thus, the HP parameter analyzer provides a bias current into the MSM at a fixed voltage (item 12 in the figure), and the measured parameter is the bias current into the MSM detector which varies as a function of the incident illumination on the MSM detector.

The laser diode driver circuit is reasonably straightforward. An amplified sine-wave generator (item 1) is input into a step-recovery-diode (SRD), (item 4) which at the correct value of input (+30dBm) will produce a continuous train of short pulses at the frequency of the sine-wave generator. The power level into the SRD is critical, if it is too low, the pulse shape is distorted and/or assymetrical, and if it is too high the SRD will fail catastrophically. If the pulse shape is poor, the laser diode (item 7) output pulse shape will also be poor, generally resulting in an inferior correlation signal. The bias-tee (item 5) combines the pulse train and DC bias signal for input into the laser diode. The DC bias signal is derived from a standard laboratory current source instrument (item 6). The value of current provided to the laser diode is set to be slightly under the lasing threshold and is therefore device dependent. Typical values of current are approximately 20 to 30 mA.

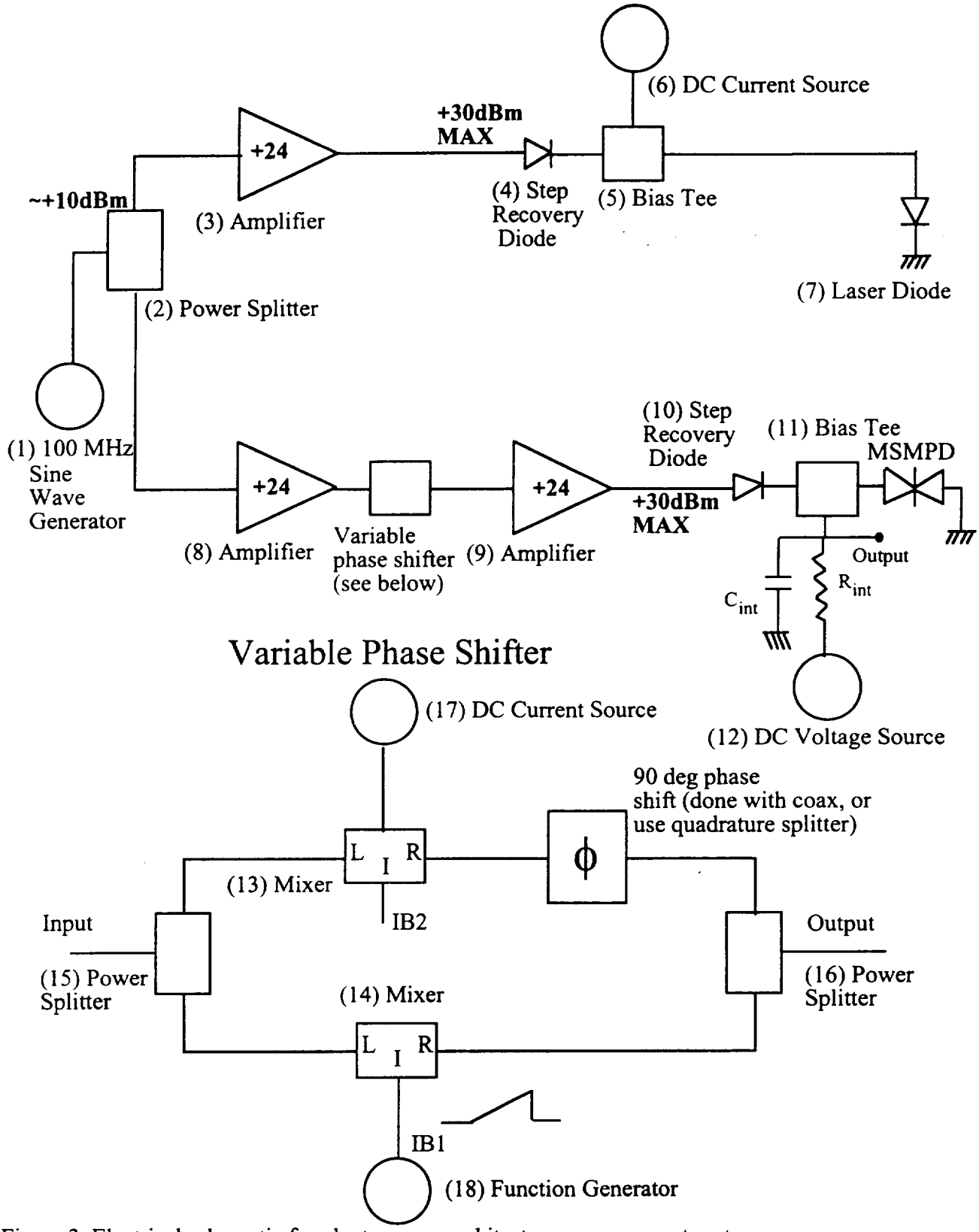

Figure 3. Electrical schematic for plant canopy architecture measurement system.

The MSM driver circuit again uses the amplified sine wave signal as an input into an SRD (item 10) to generate a train of short output pulses. These output pulses are combined with internal current source from the parameter analyzer as described above using another bias-tee (item 11).

Prior to insertion into the SRD, the sine-wave input in the MSM driver circuit is sent through a variable delay circuit as shown in the lower portion of figure 3. The variable delay circuit actually provides a variable phase shift to the input sine-wave signal, however, due to the fact that the input signal is a single frequency sine-wave, the phase shift provides the same result as an actual delay-line. At 100 MHz, the phase-shifter can provide a few nanoseconds of delay, and it is limited to 1/4 of the period of sine-wave input. The variable phase-shifter is discussed in more detail in the following section. The components and parts-lists for both driver circuits are itemized in Appendix A. It is important to note that all cable lengths which carry the high-speed signals, i.e. after the SRDs, be kept as short as possible. For the CELSS application it would be sensible to have the SRDs and all components afterwards be integrated into the remote detector head assembly.

2.2.2 Variable phase-shifter characterization

The phase shifter is composed of simple components (itemized in Appendix A), and simply adds varying proportions of a sine-wave and a cosine-wave. The varying proportions of the sine and cosine signal are controlled via the two RF mixers (items 13 and 14). By varying the amount of the DC current into the "I" port of the mixers, a proportional amount of the signal is allowed out through the "R" port. Actually, the current on one mixer is ideally held constant, while the current into the other mixer is varied linearly such as with a ramp waveform repeating at the desired frame-rate frequency. The output of one mixer is sent through a 90 degree fixed phase shift, and then the two sine-waves are now adding in quadrature.

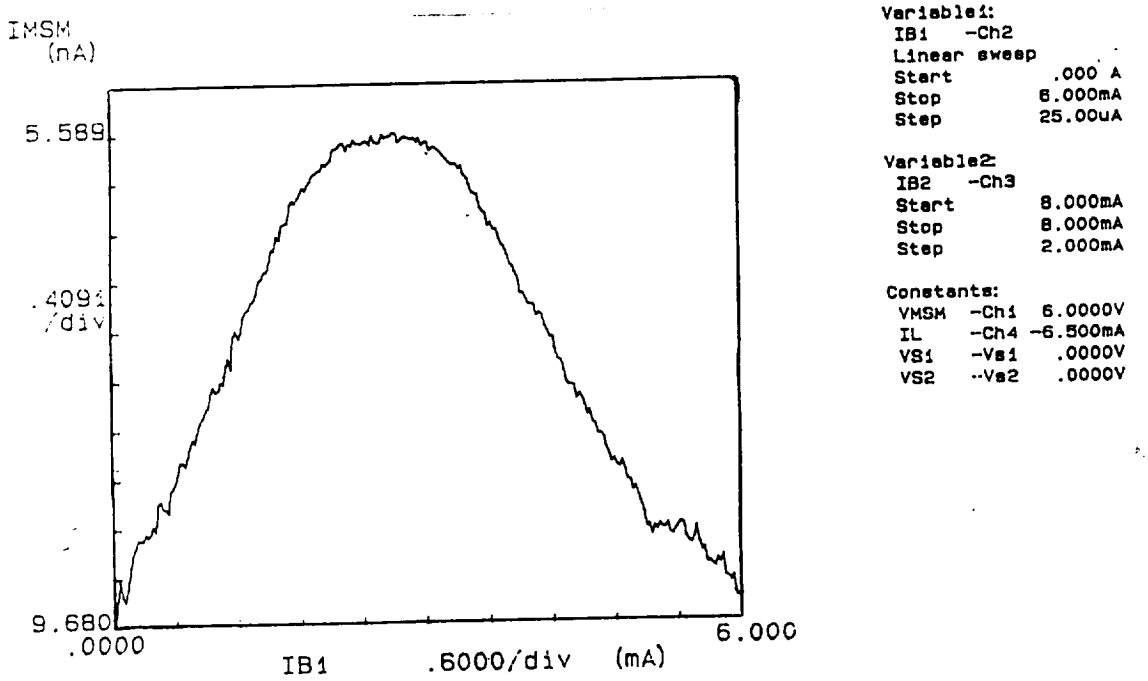

Figure 4. MSM dark current as a function of variable phase-shifter control voltage.

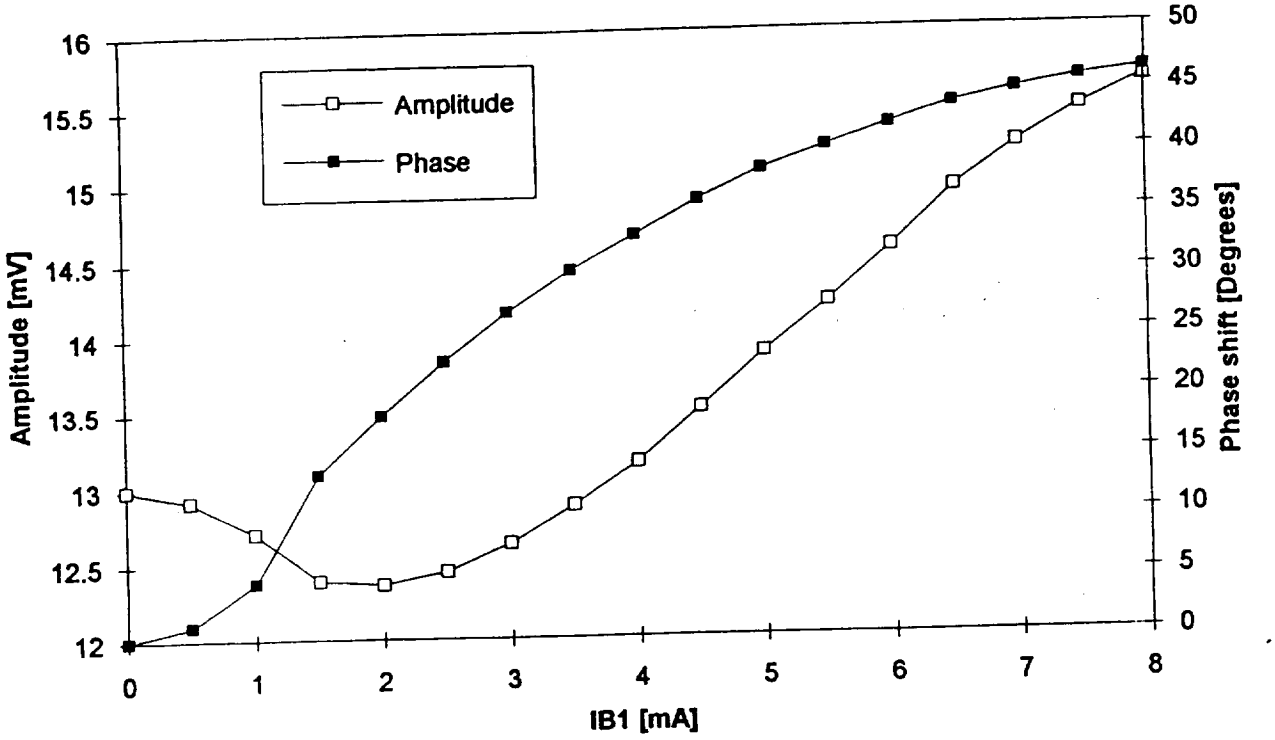

Figure 5. Voltage amplitude and phase output of variable phase-shifter plotted versus control current IB1.

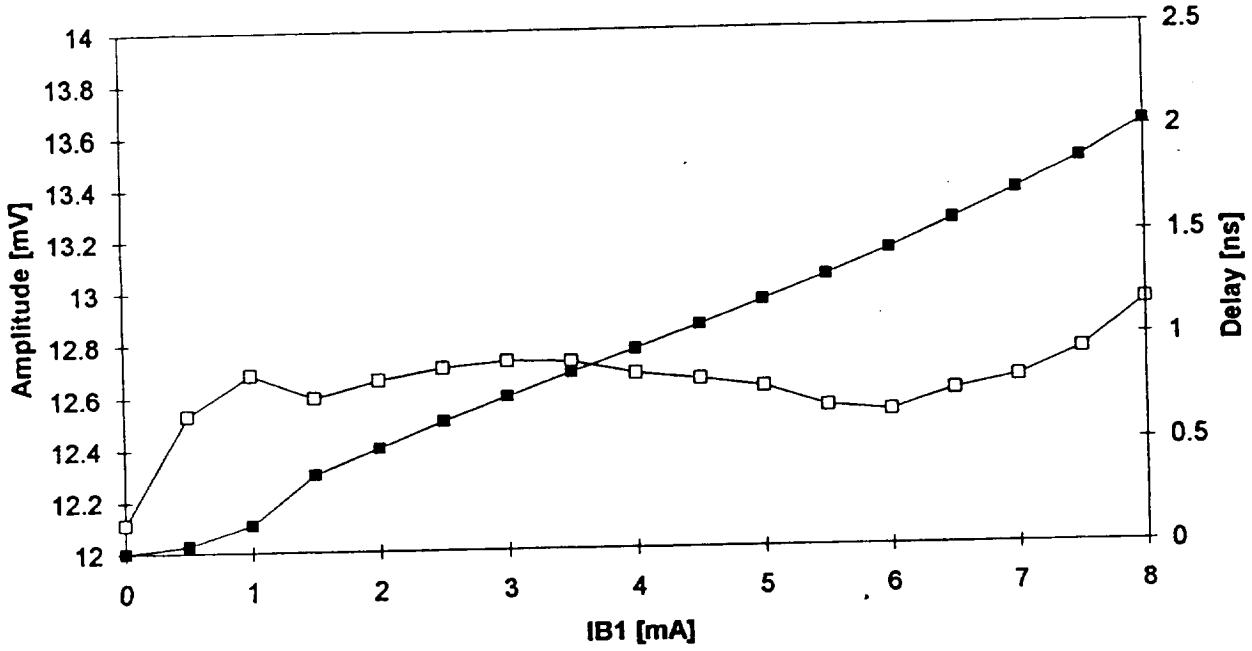

Figure 6. Voltage amplitude and temporal delay of corrected variable phase-shifter circuit plotted versus control current IB1.

The vector sum of the two quadrature signals is not linear, either in terms of amplitude or phase. The nonlinear behavior affects the quality of the correlation result in a significant manner. Ideally the phase varies linearly, and the amplitude remains constant. Having the phase vary nonlinearly is not desirable, however it can be calibrated for in the sense that the range sampling depth is simply not being sampled in a linear manner. The varying amplitude has the most deleterious effect on the correlation measurement by distorting the pulse shape and amplitude as well as contributing to an apparent nonlinear increase in the MSM dark current. The increasing dark current was observed during correlation measurements and the phase-shifter was identified as the cause by blocking the return optical pulse form hitting the detector, and observing a dramatically varying noise floor amplitude. An example of the varying dark current is shown in figure 4, where the MSM current is plotted versus the control current IB1 into one of the RF mixers. This behavior indicated that the output of the phase-shifter was not linear in amplitude.

The nonlinear behavior of the phase-shifter was confirmed by explicitly measuring the amplitude and phase of the output as IB1 was varied. The measurements are plotted in figure 5. Some initial experiments were done which varied IB2 in conjunction with IB1 so as to reduce the nonlinear behavior. To first order, this involves reducing IB2 while increasing IB1. A result is shown in figure 6, where the linearity of both the phase (converted to temporal delay here) and amplitude are dramatically improved (note the reduced amplitude scale).

3. Improving the sensitivity of the measurement system.

In addition to the improvement introduced by linearizing the phase-shifter output, several other aspects of the system have been identified, which if improved, could significantly affect measurement sensitivity. These aspects are listed below:

• Increase the laser output power. This improvement is fundamental, and would be straightforward. The current set of experiments have been done using a 670 nm laser diode with a CW power rating of 20 mW, although the average power while pulsing is only a fraction of the CW rating. Higher power laser diodes are certainly available, at least by an order of magnitude, and because the spot shape is not particularly critical for this application and direct detection is used, a stripe laser or laser diode array may be appropriate. IR and near IR lasers typically have more power, however possible multiple scattering effects in the canopy make moving to longer wavelengths less desirable.

• Use a low noise pre-amplifier at the output of the MSM. This would provide an immeadiate signal-to-noise improvement for the receiver.

• Use a lock-in amplifier at the receiver. A low frequency modulation (tens of kHz) on the bias current for the laser diode provides a modulation which can be used for detection by a lock-in amplifier. Experiments have been done with a demonstrated improvement greater than an order of magnitude.

• Reduce internally reflected pulses from MSM to SRD. At high frequencies (tens of GHz) the impedance of the MSM is a few hundred Ohms, and therefore there is an impedance mismatch between the MSM and the SRD. Thus, the input pulse into the MSM is partially reflected back towards the SRD, and back to the MSM, and so-on. The reflected pulses result in a distorted pulse which affects the correlation measurement. Placing an attenuator in between the SRD and the MSM to act as a double-pass attenuation greatly reduces the power of the multiply reflected pulses. For example, placing a 6 dB attenuator in between the SRD and the MSM would reduce the first doubly-reflected pulse by 12 dB compared to the forward going pulse.

• Reduce the dark-current of the MSM detector. MSM detectors used in the setup at CU had a leakage current larger than 1 μA due to application of high voltages (> 5 V) during setup and testing. While these detectors still enabled operation of the system at a range of 0.5 - 1 meter, a 10 nA dark current would furture reduce the noise floor by 10 dB.

4. Delivered Detectors

We have provided 6, single MSM photodetectors mounted in high-speed packages as deliverables for this contract. The detectors have been shipped directly to Dr. Vern C. Vanderbilt, at NASA Ames Research Center. The high-speed package design will not compromise the performance of the device, as confirmed up to bandwidths in excess of 5 GHz at The Unversity of Colorado. Detailed documentation regarding the detectors is provided in Appendix B.

Appendix A

Thor Labs
(201) 579-7227
Melles-Griot
1-800-835-2626
Optics Parts List for MSM/CELSS Sensor
(TH) means thorlab, all others melles-griot. *items are not for designs 1 or 2

DESCRIPTION	MODEL	PAGE	QTY	PRICE/PER	TOTAL
Aspheric lens;f=18mm, dia=24mm, AR coat	01LAG005/066	9-4	3	$27.50	$82.50
*Aspheric lens;f=33mm, dia=52mm, AR coat	01LAG010/066	9-4	2	$69.10	$138.20
*Aspheric lens;f=25mm, dia=32.5mm, AR coat	01LAG117/066	9-4	2	$44.10	$88.20
Bi-convex lens;f=20mm, dia=21mm AR coat	01LDX027/066	5-9	1	$40.40	$40.40
Bi-convex lens;f=25.4mm, dia=20mm AR coat	01LDX041/066	5-9	1	$38.50	$38.50
*Bi-convex lens;f=10mm, dia=10mm AR coat	01LDX009/066	5-9	1	$29.50	$29.50
*Bi-convex lens;f=15mm, dia=14.5mm AR coat	01LDX019/066	5-9	1	$31.10	$31.10
*Bi-convex lens;f=30mm, dia=22.4mm AR coat	01LDX055/066	5-9	1	$39.50	$39.50
Mirror; 12.5mm square,HR coat (MG)	02MFG000/023	12-12	2	$57.00	$114.00
Mirror; 25mm square,HR coat (MG)	02MFG001/023	12-12	2	$65.00	$130.00
Collimating Lens;f=8mm, NA=0.50	C240TM-B (TH)	46	1	$73.60	$73.60
Collimating Lens;f=6.24mm, NA=0.40	C110TM-B (TH)	46	1	$73.60	$73.60
*Collimating Lens;f=6.16mm, NA=0.30	C170TM-B (TH)	46	1	$74.80	$74.80
Collimation Tube	LT240A (TH)	49	1	$21.00	$21.00
Collimation Tube	LT110A (TH)	49	1	$21.00	$21.00
Laser Diode;20mW, 670nm	CQL806/D (TH)	37	1	$183.00	$183.00
SUBTOTAL					**$1,178.90**

	Electrical Component	Parts List		
	MC:Mini-circuits 800-654-7949			
	HP:800-452-4844			
	PPL:Picosecond-Pulse-Labs:			
	303-443-1249			
	JFW:317-887-1340			
Item	**Description**	**Manuf/Part#**	**Price**	Optional Price
1	Signal Generator; >100 MHz, 10 dBm	not specified	0	
2	RF Power Splitter	MC/ZSC-2-1	27.95	
3	RF Power Amp; +24dB, 10-1200 MHz	MC/ZHL-2-12	625	
3-opt	RF Power Amp; +25dB, .05-130 MHz	MC/ZHL-32A	0	199
4	Step Recovery Diode	HP/33002A	375	
5	Bias-Tee; 100KHz-18GHz, tr=20ps	PPL/5550B	250	
6	DC Current Source	not specified	0	
7	Laser Diode	see optics list	0	
8	RF Power Amp; +24dB, 10-1200 MHz	MC/ZHL-2-12	625	
8-opt	RF Power Amp; +25dB, .05-130 MHz	MC/ZHL-32A	0	199
9	RF Power Amp; +24dB, 10-1200 MHz	MC/ZHL-2-12	625	
9-opt	RF Power Amp; +25dB, .05-130 MHz	MC/ZHL-32A	0	199
10	Step Recovery Diode	HP/33002A	375	
11	Bias-Tee; 100KHz-18GHz, tr=20ps	PPL/5550B	250	
12	DC Voltage Source	not specified		
13	Mixer	ZAY-1	64.95	
14	Mixer	ZAY-1	64.95	
15	Power Splitter	ZSC-2-1	27.95	
16	Power Splitter	ZSC-2-1	27.95	
17	DC current Source	not specified	0	
18	Function Generator	not specified	0	
19	Fixed Attenuator 3dB (Set of 2)	MC/SAT-3	42	
20	Fixed Attenuator 6dB (Set of 2)	MC/SAT-6	42	
21	Fixed Attenuator 10dB (Set of 2)	MC/SAT-10	42	
22	Variable Attenuator (0-45 dB)	JFW/50B-001	138	
	Total		3602.7	
	Total (using optional items)		2324.7	

Appendix B

Description of deliverables (6 packaged MSM photodetectors)

Note: 6 packaged single detectors, rather than the 2 packaged two-dimensional detector arrays listed in the contract. The single detectors were specifically requested by Dr. Vanderbilt.

Detector description

The detectors consist of Chrome/Gold electrodes on a Gallium Arsenide (GaAs) epitaxially grown layer. Interdigitated 3 μm wide electrodes (fingers) with 3 μm spacing cover the 100 μm x 100 μm photosensitive area. The fingers are connected to two bonding pads through which the detector is electrically connected to a high-speed SMA connector. The detectors are mounted in a high-speed package and are protected by a glass cover. A 1/16" tap is provided for easy positioning on an optical bench. A drawing of the package and a picture of a 100 x 100 μm^2 detector is shown below:

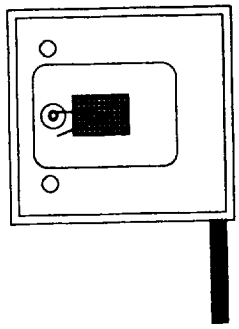

FRONT VIEW

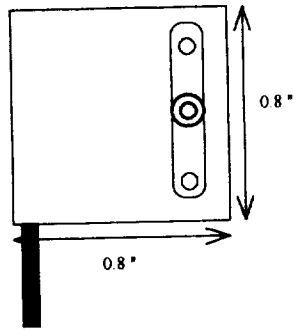

BACK VIEW

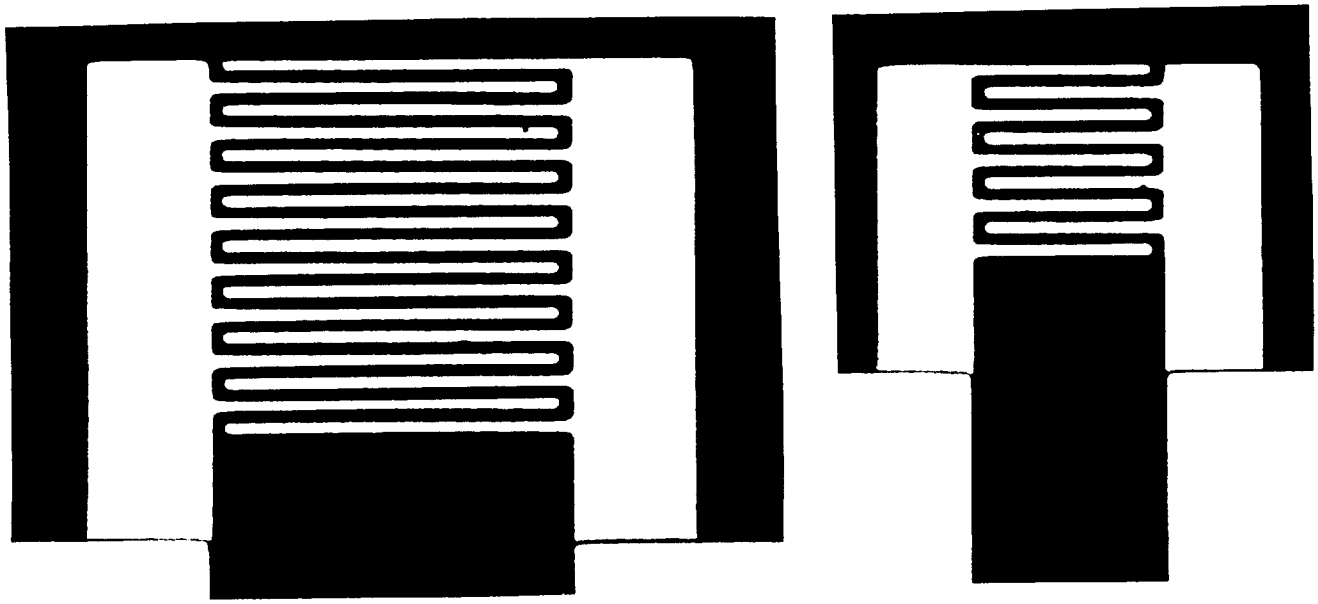

Picture of a 100 x 100 μm^2 (left) and a 50 x 50 μm^2 (right) MSM detector

Detector operation

NOTE: the detectors are high-speed components which are sensitive to electro-static discharges. Use of ground straps is required unless the detectors are connected to a low resistance (< 1 kΩ).

Detector biasing

The detectors can operate with a positive as well as with a negative bias voltage ranging from -5 to 5 Volt. Actual responsivity and dark current characteristics are shown below for each detector. Care should be taken so that the applied voltage is never outside this range even for short periods of time. Power supply transients and application of short electrical pulses (20 ps or longer) with a peak amplitude larger than 5 Volt should be avoided.

Current limiting

The detectors should not be operated at currents larger than 1 mA, which could occur when applying optical power in excess of 10 mW. Use of a current limiting circuit is recommended, while special care should be used when applying short electrical pulses so that the average current does not exceed 1 mA for 10 ns or longer.

Detector operation and handling

While the detectors are protected with a glass cover to prevent damage to the detectors and bondwires, the package is not hermetically sealed. Therefore the detectors should not be operated in humid environments, nor should they be cooled below ambient temperature to avoid condensation within the package.

Additional remarks

The detectors have a very low dark current and are sensitive to ambient light. They should be shielded from room light for best performance.

The detectors are sensitive to light outside the photosensitive area, but have a much longer pulse response in this mode due to the longer transit time of the carriers. Therefore, for best high-speed performance one should uniformely illuminate the area covered by the fingers.

Measured data

Attached are current-voltage characteristics measured from -5 Volt to 5 Volt four all detectors. Four curves are measured when illuminating the detector using a monochromatic light source (λ = 670 nm). Each curve corresponds to a different incident power namely 0 μW, 1.4 μW, 3.8 μW and 8.4 μW. A plot of the dark-current versus voltage on an expanded scale is also provided for each detector.

The individual detectors are labeled with the letters B, C, D, G, H and I. Detectors B, C, D, H and I have a photosensitive area of 100 μm by 100 μm and contain 17 fingers, while detector G has a photosensitive area of 50 μm by 50 μm and contains 9 fingers.

The detectors have a responsivity at 670 nm wavelength of 100 ± 6 nA/μW and a leakage current below 25 nA when biased between -5 and 5 Volt. The responsivity was measured at 5 Volt while illuminating about half of the detector area containing the fingers

Careful handeling and biasing will preserve the low leakage current of the detector, while exceeding the specific biasing conditions will cause the dark current to slowly increase over time.

The best system performance is expected when using detectors B, C, and D. Detectors H and I are equivalent but have a higher leakage current which is expected to raise the noise floor by 2 dB. Detector G and H are recommended to set up and test the overall system.

Detector Label	Size [μm^2]	Dark current [nA]	Responsivity at 670 nm [nA/μW]
B	100 x 100	6.9	102
C	100 x 100	9.6	100
D	100 x 100	7.9	95
G	50 x 50	23.8	96
H	100 x 100	16.8	105
I	100 x 100	12.5	94

****** GRAPHICS PLOT ******

MSM CHIP B

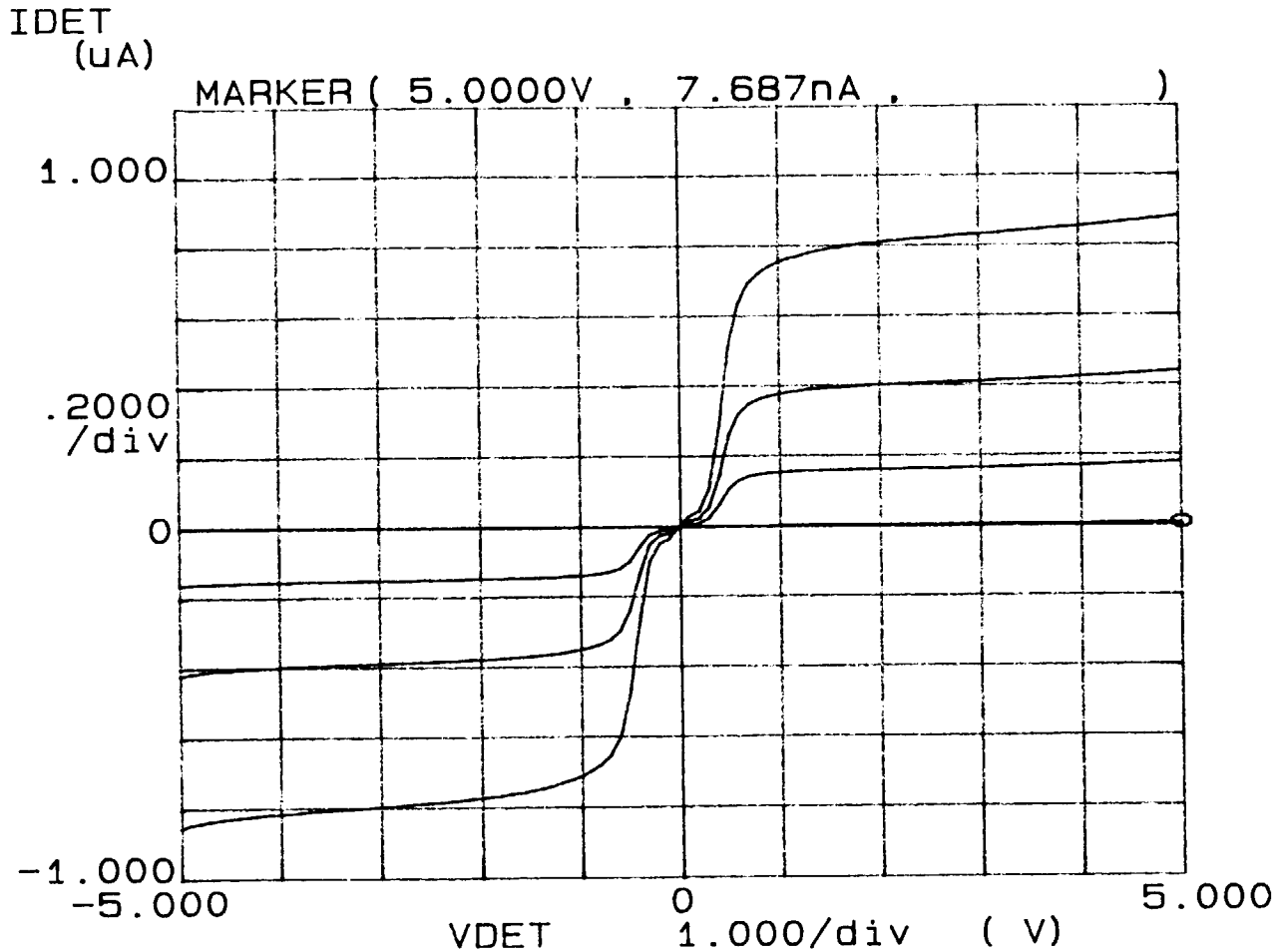

Variable1:
VDET -Ch3
Linear sweep
Start -5.0000V
Stop 5.0000V
Step .1000V

Variable2:
IL -Ch2
Start .000 A
Stop -36.00mA
Step -12.00mA

Constants:
GND -Ch1 .0000V

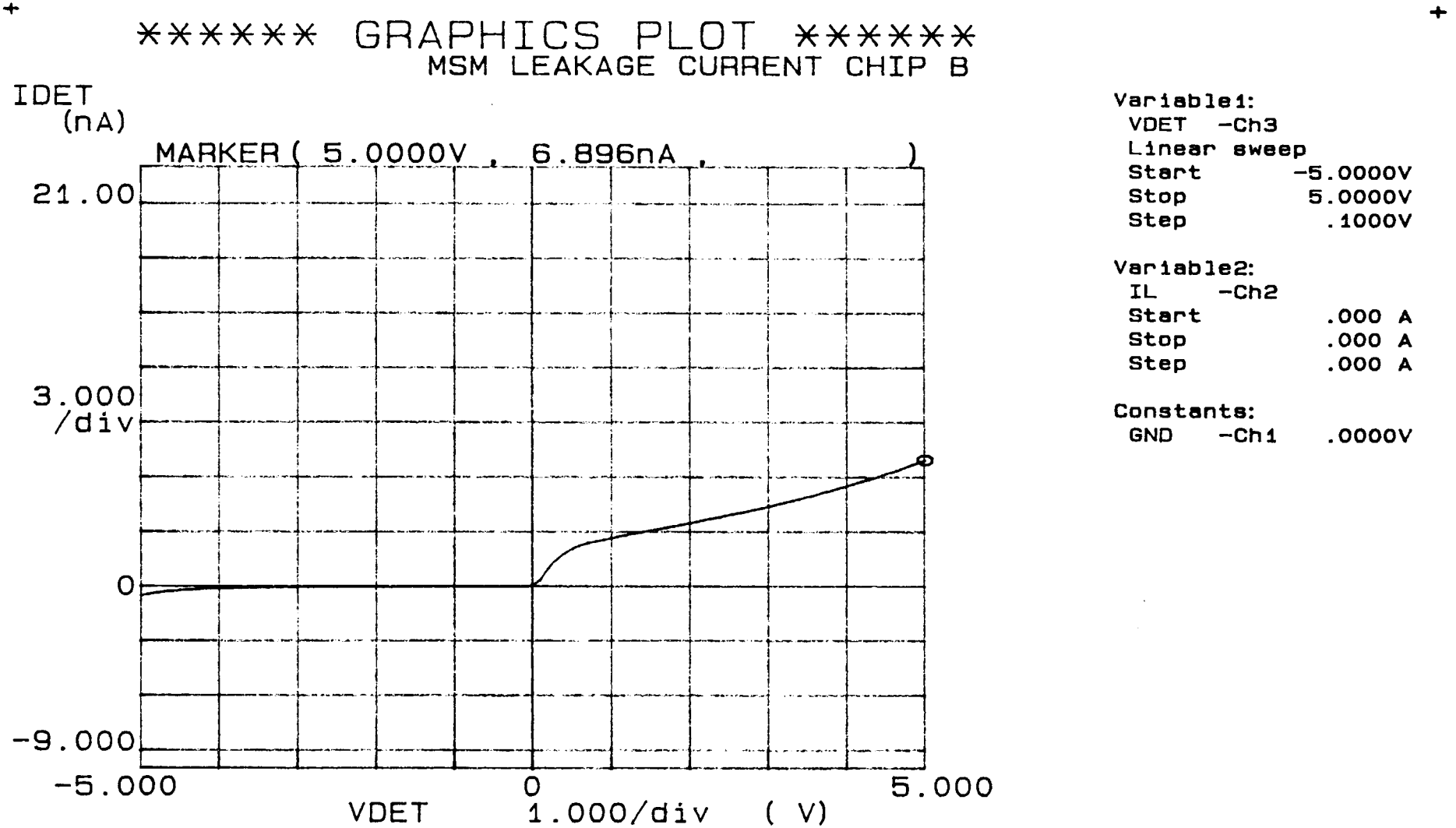
****** GRAPHICS PLOT ******
MSM LEAKAGE CURRENT CHIP B
IDET
(nA)
MARKER (5.0000V , 6.896nA ,)
21.00
3.000
/div
0
-9.000
-5.000
0
5.000
VDET
1.000/div
(V)
Variable1:
VDET -Ch3
Linear sweep
Start -5.0000V
Stop 5.0000V
Step .1000V
Variable2:
IL -Ch2
Start .000 A
Stop .000 A
Step .000 A
Constants:
GND -Ch1 .0000V

****** GRAPHICS PLOT ******

MSM CHIP C

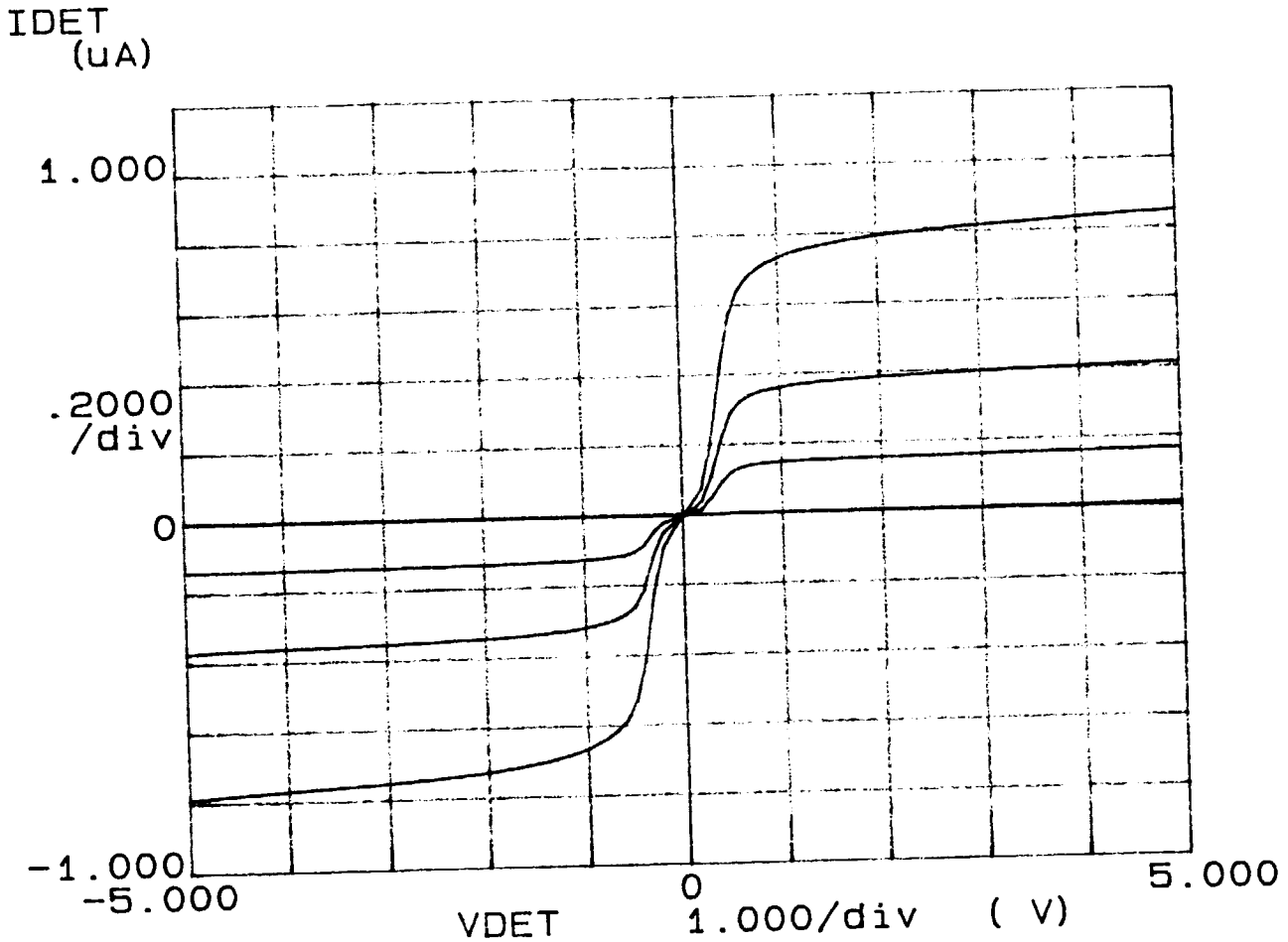

Variable1:
VDET -Ch3
Linear sweep
Start -5.0000V
Stop 5.0000V
Step .1000V

Variable2:
IL -Ch2
Start .000 A
Stop -36.00mA
Step -12.00mA

Constants:
GND -Ch1 .0000V

****** GRAPHICS PLOT ******

MSM LEAKAGE CURRENT CHIP C

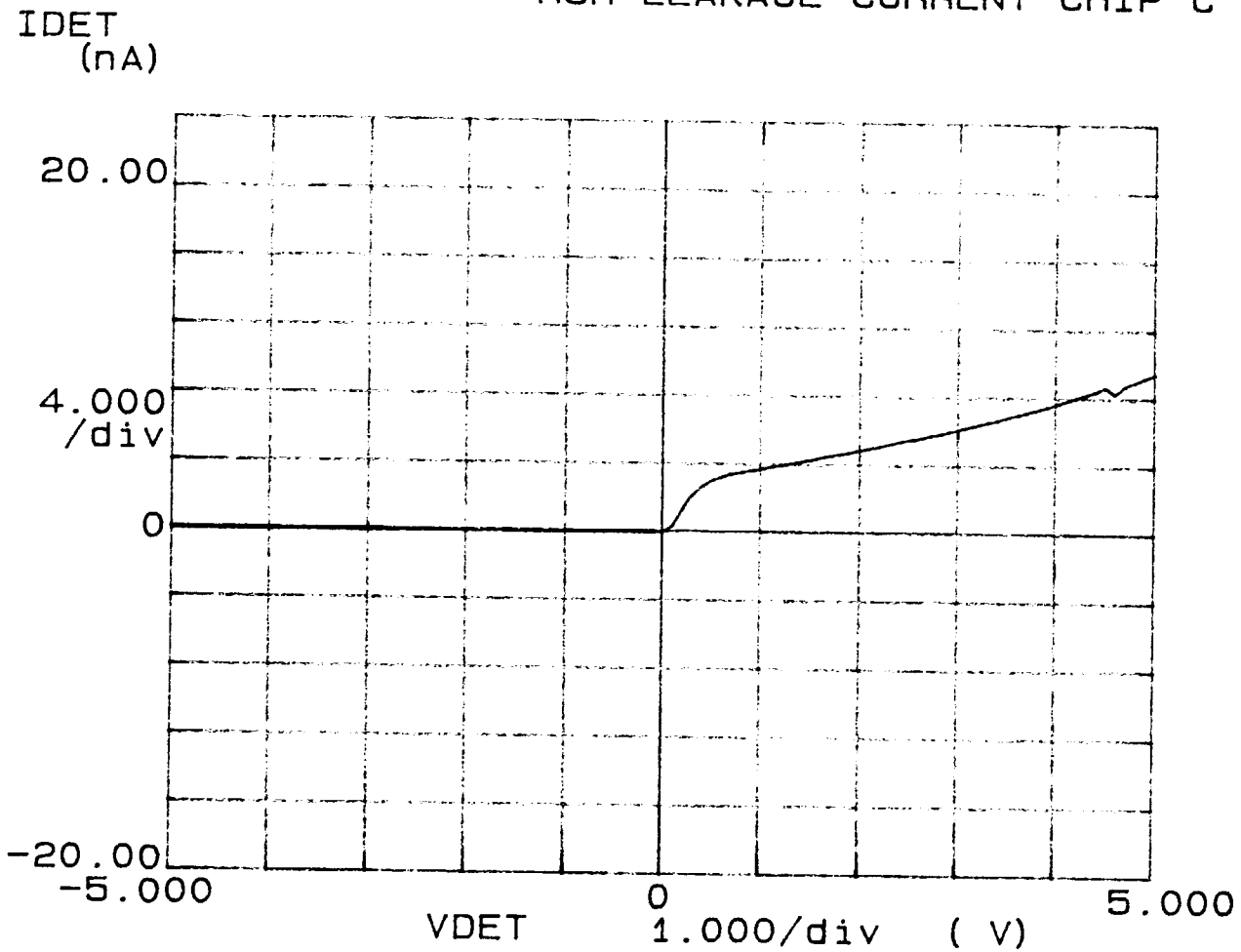

Variable1:
VDET -Ch3
Linear sweep
Start -5.0000V
Stop 5.0000V
Step .1000V

Variable2:
IL -Ch2
Start .000 A
Stop .000 A
Step .000 A

Constants:
GND -Ch1 .0000V

****** GRAPHICS PLOT ******

MSM CHIP D

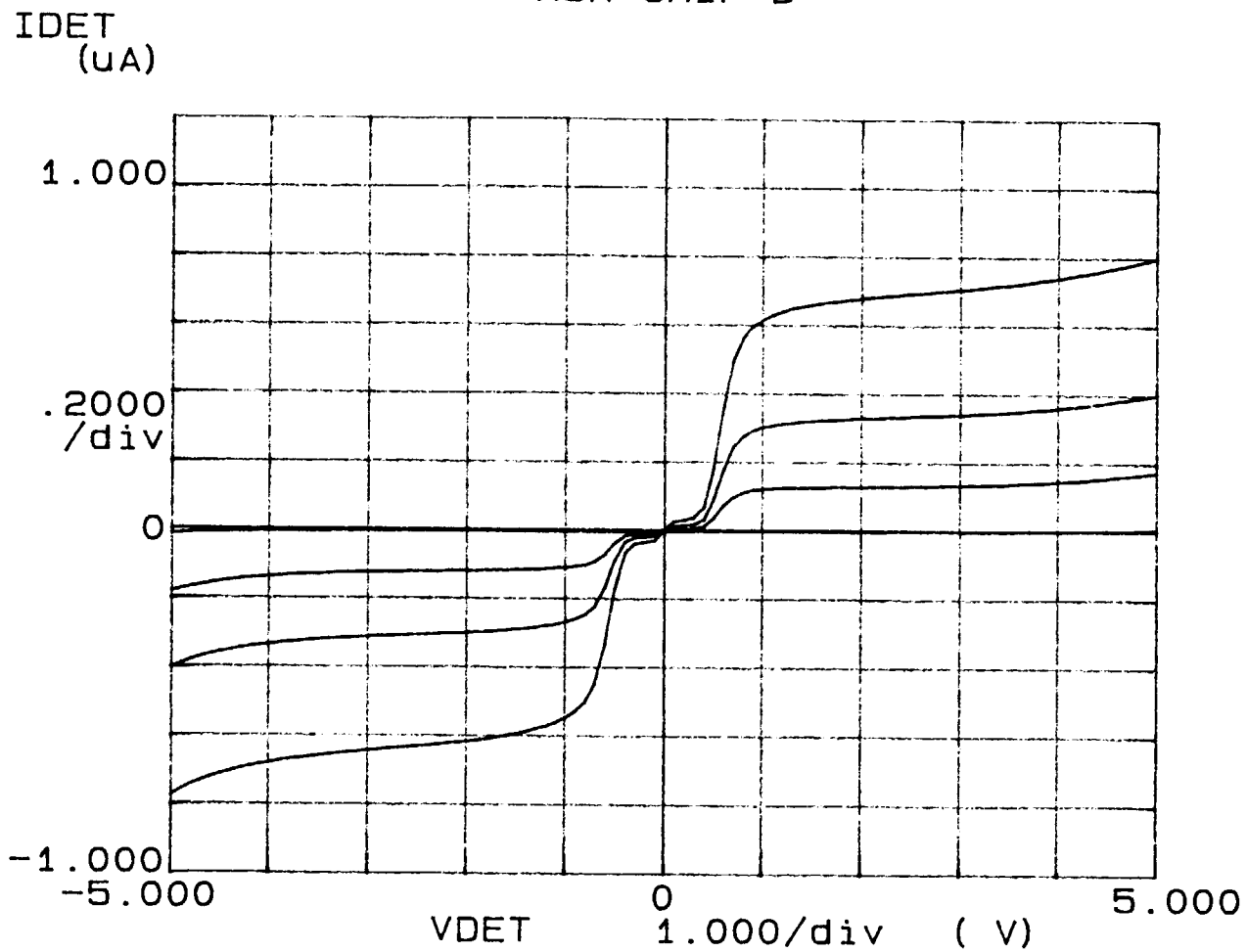

Variable1:
VDET -Ch3
Linear sweep
Start -5.0000V
Stop 5.0000V
Step .1000V

Variable2:
IL -Ch2
Start .000 A
Stop -36.00mA
Step -12.00mA

Constants:
GND -Ch1 .0000V

****** GRAPHICS PLOT ******

MSM LEAKAGE CURRENT CHIP D

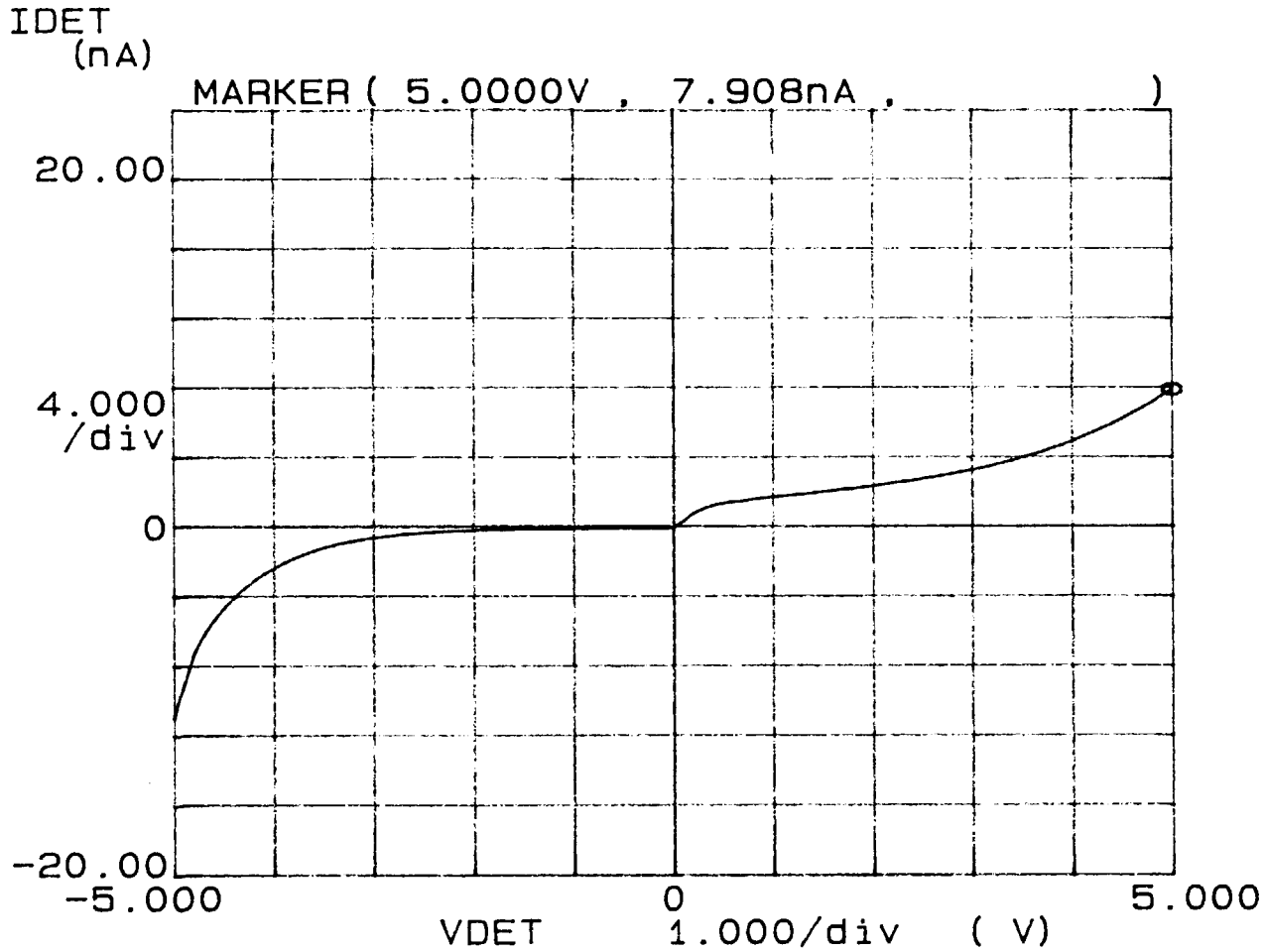

Variable1:
VDET -Ch3
Linear sweep
Start -5.0000V
Stop 5.0000V
Step .1000V

Variable2:
IL -Ch2
Start .000 A
Stop .000 A
Step .000 A

Constants:
GND -Ch1 .0000V

****** GRAPHICS PLOT ******

MSM CHIP G

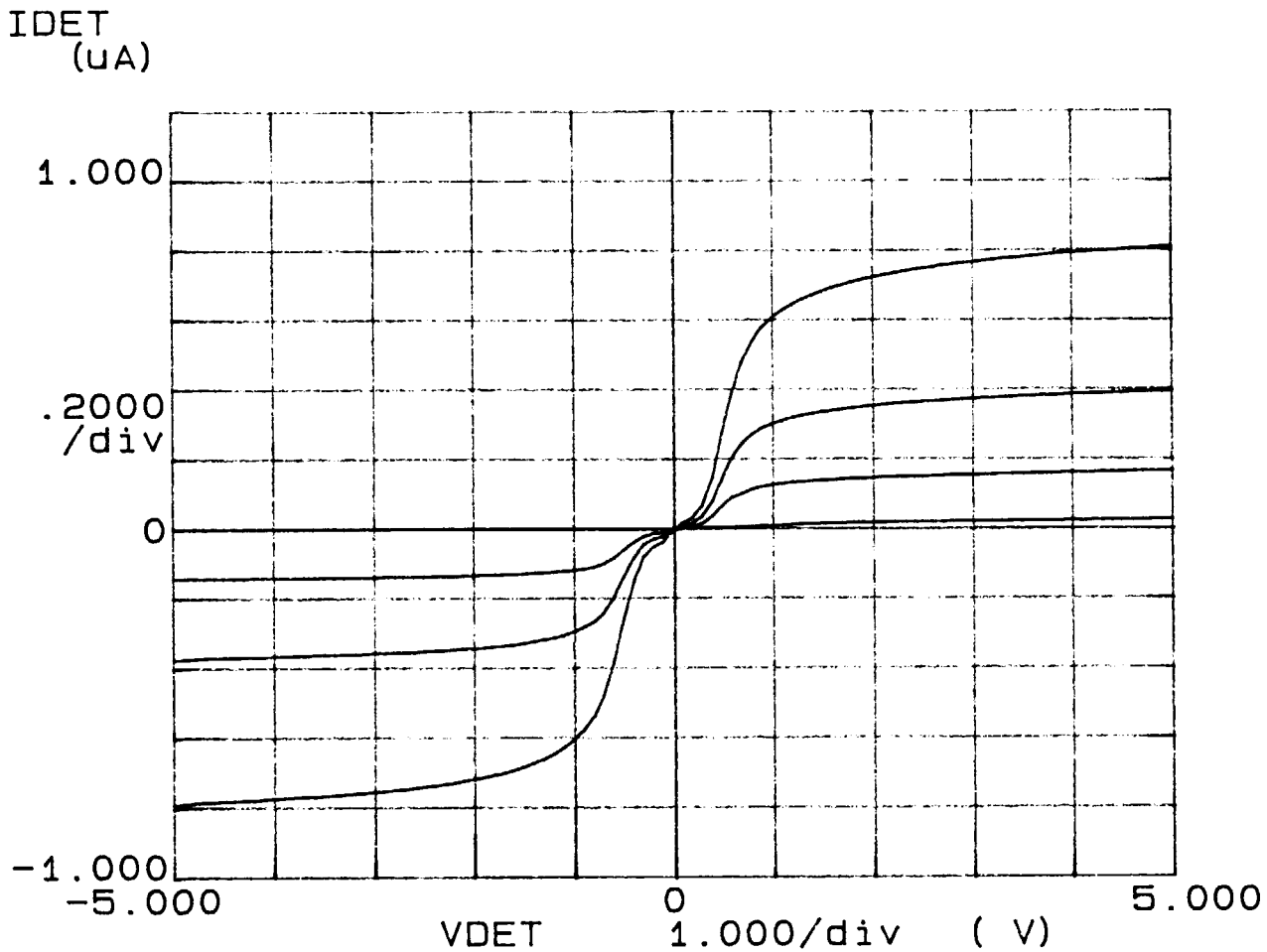

Variable1:
VDET -Ch3
Linear sweep
Start -5.0000V
Stop 5.0000V
Step .1000V

Variable2:
IL -Ch2
Start .000 A
Stop -36.00mA
Step -12.00mA

Constants:
GND -Ch1 .0000V

****** GRAPHICS PLOT ******

MSM LEAKAGE CURRENT CHIP G

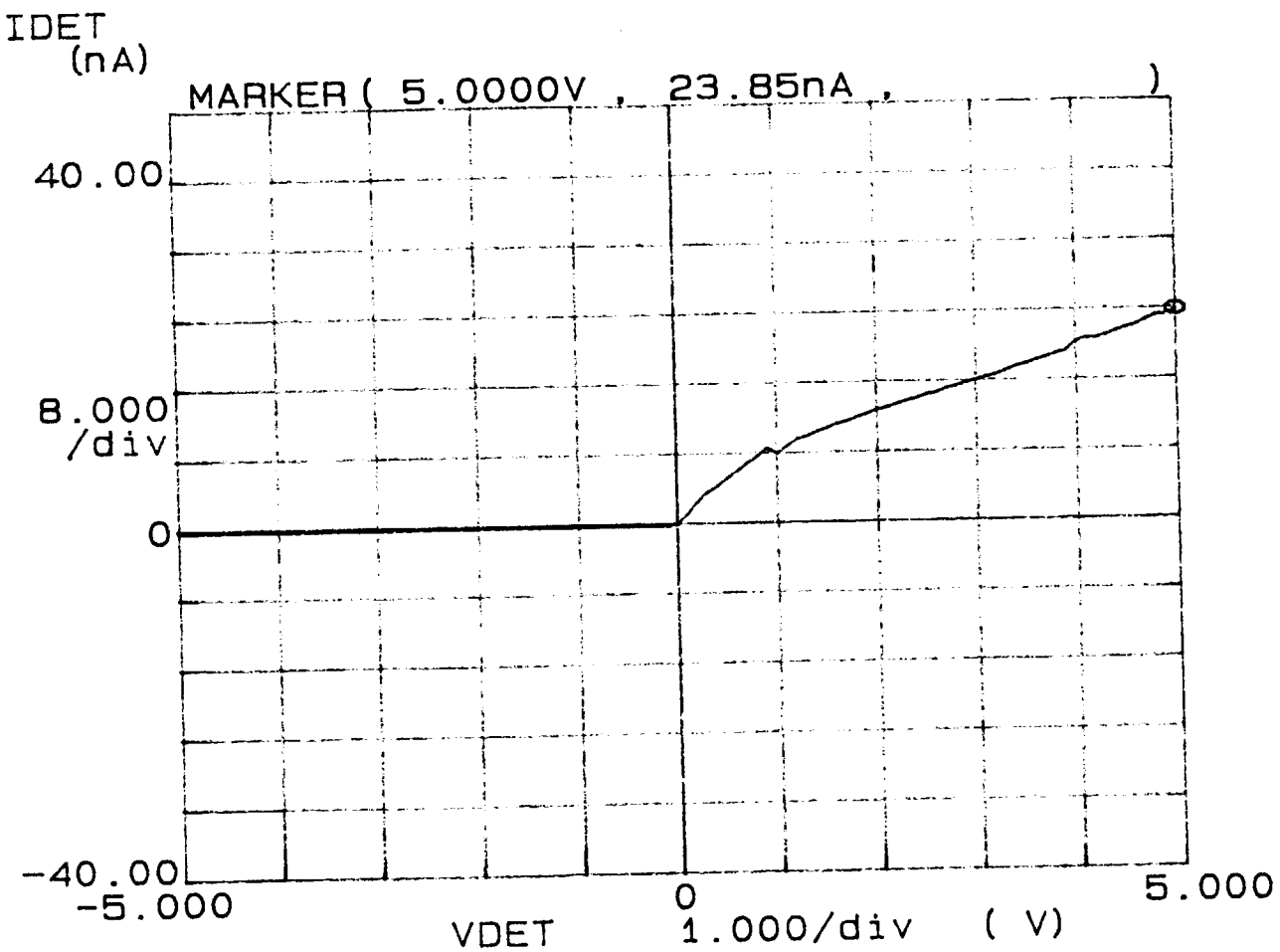

Variable1:
VDET -Ch3
Linear sweep
Start -5.0000V
Stop 5.0000V
Step .1000V

Variable2:
IL -Ch2
Start .000 A
Stop .000 A
Step .000 A

Constants:
GND -Ch1 .0000V

****** GRAPHICS PLOT ******

MSM CHIP H

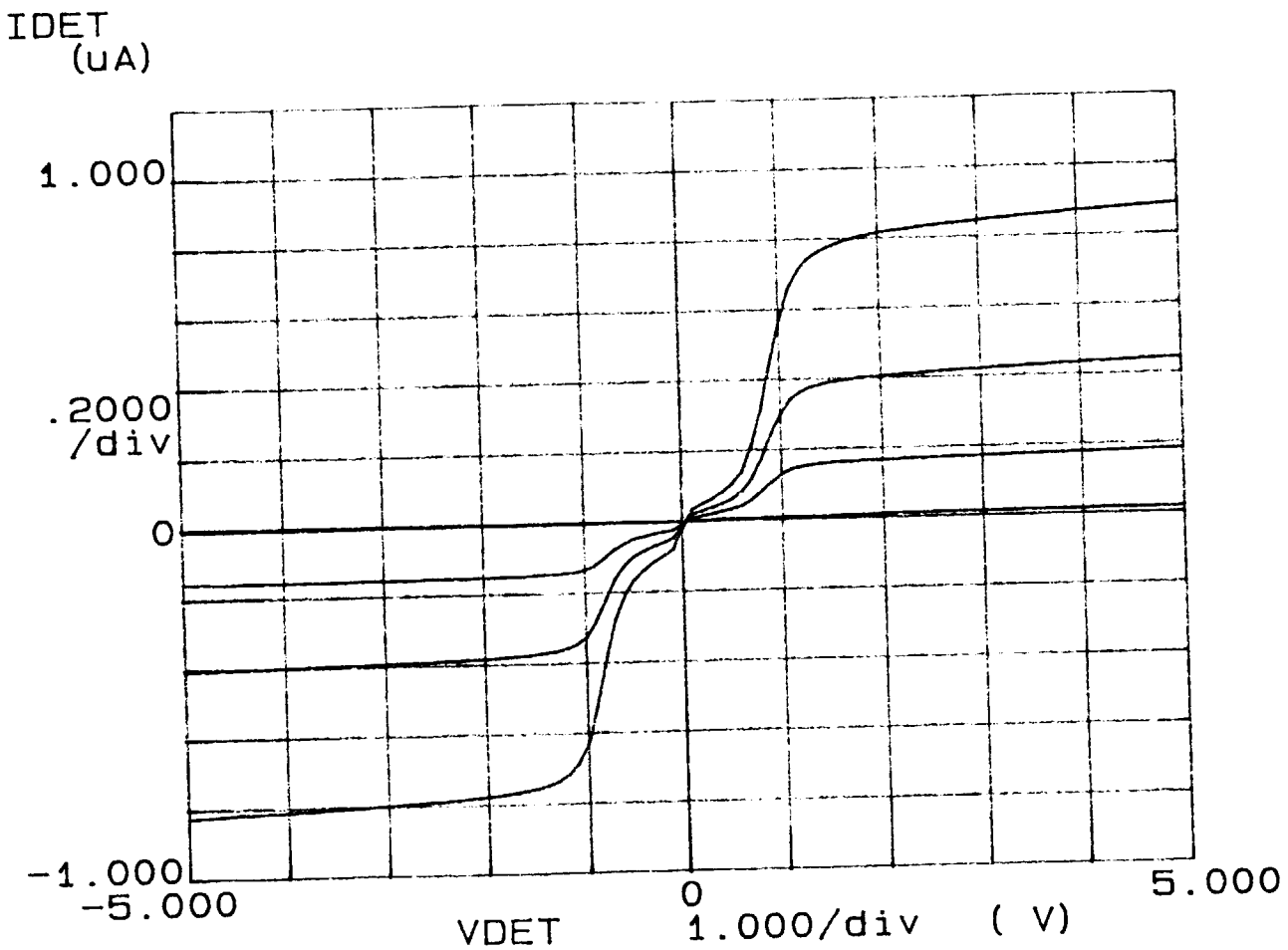

Variable1:
VDET -Ch3
Linear sweep
Start -5.0000V
Stop 5.0000V
Step .1000V

Variable2:
IL -Ch2
Start .000 A
Stop -36.00mA
Step -12.00mA

Constants:
GND -Ch1 .0000V

****** GRAPHICS PLOT ******

MSM LEAKAGE CURRENT CHIP H

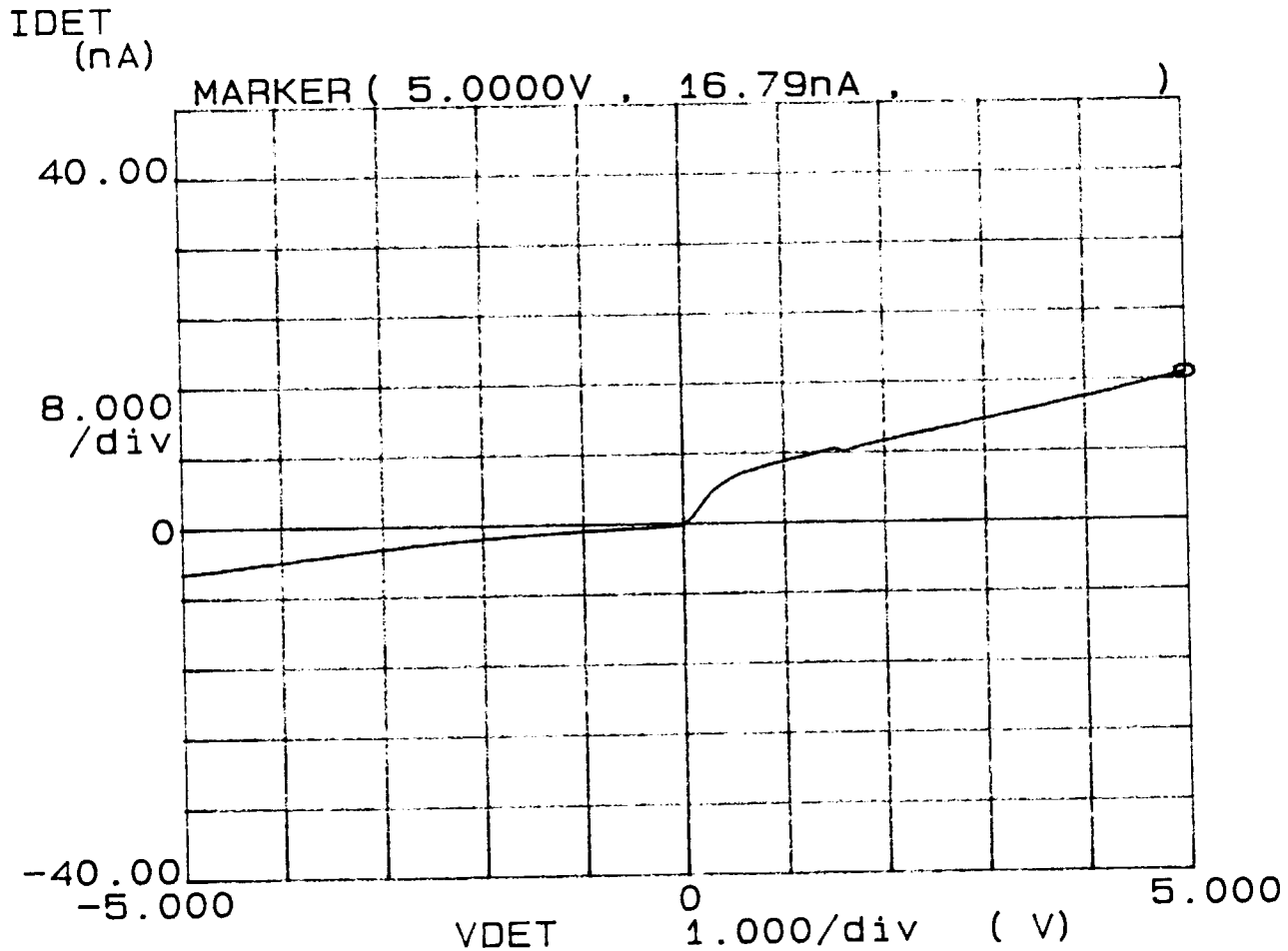

Variable1:

VDET -Ch3	
Linear sweep	
Start	-5.0000V
Stop	5.0000V
Step	.1000V

Variable2:

IL -Ch2	
Start	.000 A
Stop	.000 A
Step	.000 A

Constants:

GND	-Ch1	.0000V

****** GRAPHICS PLOT ******

MSM CHIP I

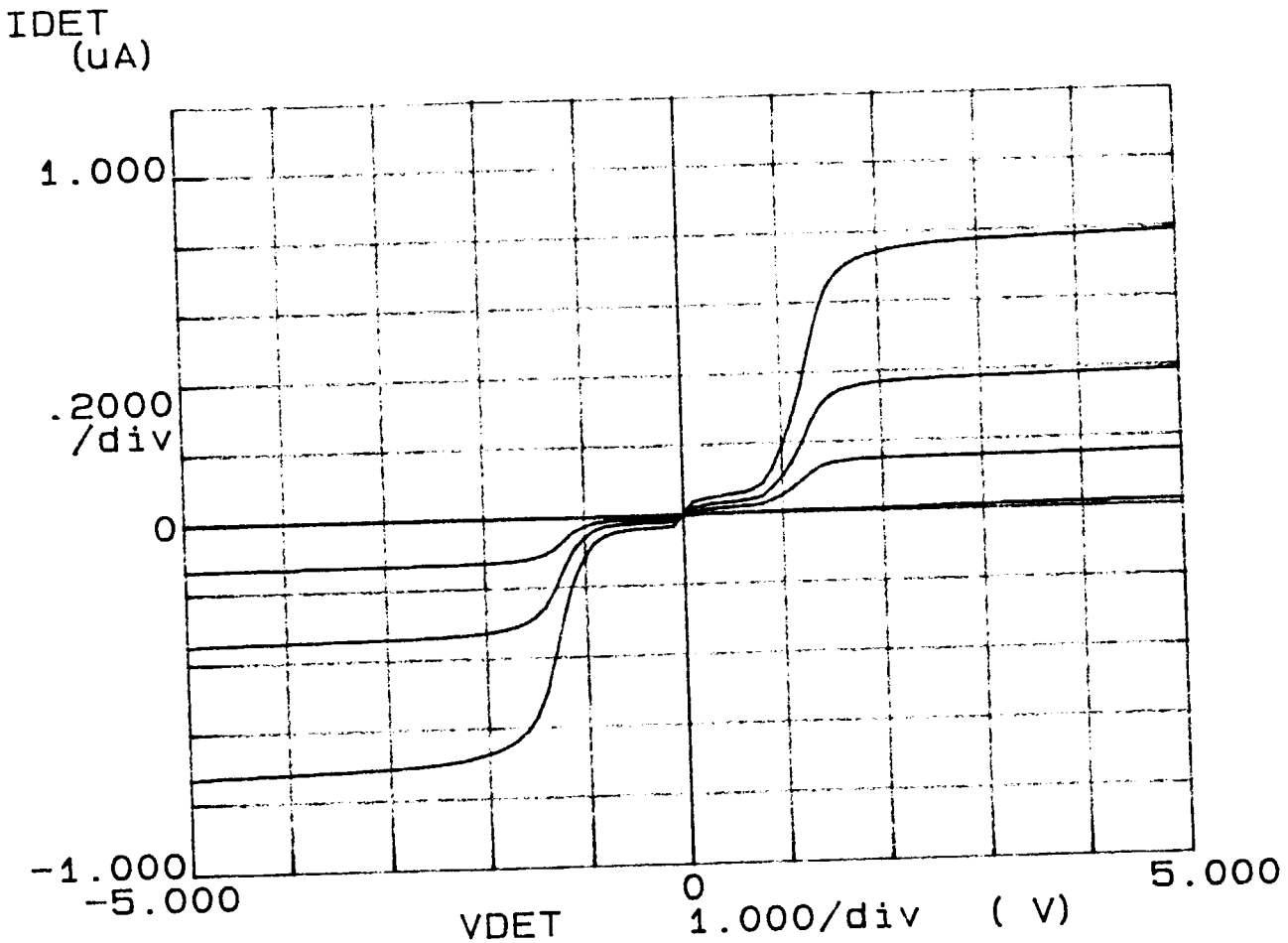

Variable1:
VDET -Ch3
Linear sweep
Start -5.0000V
Stop 5.0000V
Step .1000V

Variable2:
IL -Ch2
Start .000 A
Stop -36.00mA
Step -12.00mA

Constants:
GND -Ch1 .0000V

****** GRAPHICS PLOT ******

MSM LEAKAGE CURRENT CHIP I

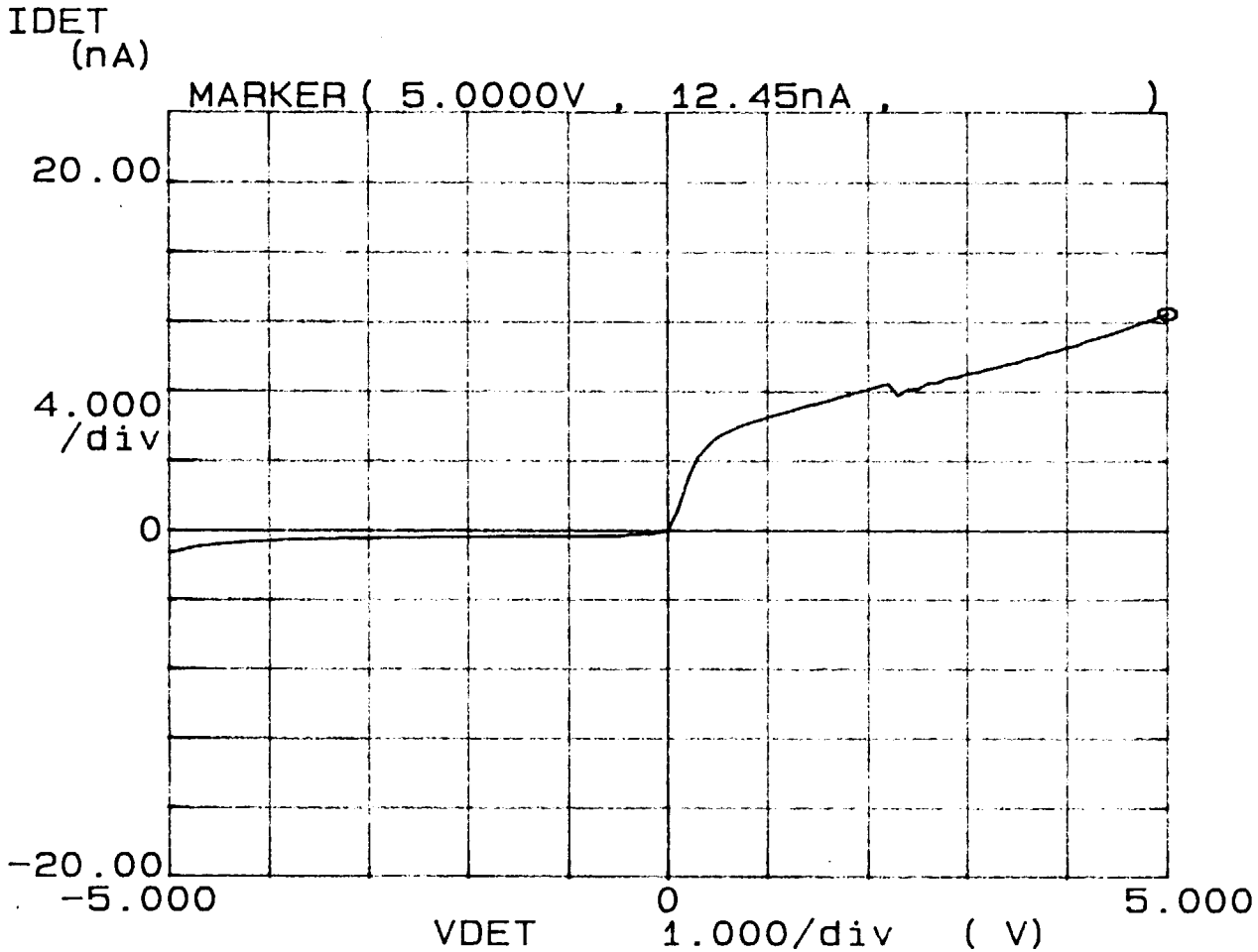

Variable1:
VDET -Ch3
Linear sweep
Start -5.0000V
Stop 5.0000V
Step .1000V

Variable2:
IL -Ch2
Start .000 A
Stop .000 A
Step .000 A

Constants:
GND -Ch1 .0000V